# Geochronological and Geochemical Study of Zircon from Tourmaline-Muscovite Granites of the Archaean Kolmozero–Voronya Greenstone Belt: Insights into Sources of the Rare-Metal Pegmatites

**Nikolay M. Kudryashov [1,\*], Oksana V. Udoratina [2], Matthew A. Coble [3] and Ekaterina N. Steshenko [1]**

1   Geological Institute of Kola SC RAS, 184209 Apatity, Russia; steshenko@geoksc.apatity.ru
2   Institute of Geology of Komi SC UB RAS, 167982 Syktyvkar, Russia; udoratina@geo.komisc.ru
3   Department of Geological Sciences, Stanford University, Stanford, CA 94305, USA;
    matthew.coble@gmail.com
\*   Correspondence: nik@geoksc.apatity.ru

**Abstract:** In order to determine the U-Pb crystallization age of zircon from the tourmaline-muscovite granites of the Kolmozero–Voronya greenstone belt located in the northeastern Fennoscandian Shield (Kola Peninsula), an isotope-geochronological study of the zircon grains was performed using a SHRIMP-RG microprobe. The belt is represented by the Archaean volcano-sedimentary rocks (2.9–2.8 Ga). Deposits of rare-metal pegmatites (Li and Cs with associated Nb, Ta, and Be) occur within the belt and on its margins. The age of the pegmatites within the belt was estimated at 2.7–2.6 Ga. Until now, there has been no generally accepted view on the genetic relation of the pegmatites with granite. Various authors have suggested that the pegmatites could potentially be associated with many type of granitoids within the region, i.e., plagiogranites, tonalites, amphibole-biotite granodiorites, microcline granites, alkaline granites, or muscovite-tourmaline granites. Zircon crystals from the muscovite-tourmaline granites are heterogeneous; they have less altered cores and strongly altered rims. The zircon cores are slightly enriched in U at a value of 173–1030 ppm, Th/U = 0.1–0.4. The zircons' rims are heavily enriched in U at a value of 700–3300 ppm, Th/U = 0.03–0.08, indicating metasomatic processes. Zircon characteristics show that it crystallized from a melt enriched in a fluid phase. Fluid activity lasted after zircon crystallization as reflected in the irregular composition of the mineral and its rare earth element (REE) patterns that are typical of a metasomatic zircon. The computed zircon crystallization temperature in the tourmaline-muscovite granites is in the range of 650–850 °C. The discordant age calculated for five analyzed points of the zircon crystal cores is 2802 ± 13 Ma. The discordant age for four analyzed points of the zircon crystal rims is found to be 2728 ± 14 Ma. On the basis of the obtained isotope-geochronological data, we conclude that the tourmaline-muscovite granites located in the immediate vicinity of rare-metal pegmatite veins are the most probable source of matter for the pegmatites.

**Keywords:** Archaean tourmaline-muscovite granite; U-Pb (SHRIMP) zircon; Kolmozero spodumene pegmatite deposit; Kola Peninsula

## 1. Introduction

The emplacement of granite pegmatites in the Earth's history started at the earliest stages of its evolution [1–3]. Rare-metal pegmatites typically exhibit their confinement to Precambrian greenstone belts striking along ancient deep-seated faults. The idea of a genetic link between the

rare-metal pegmatites and granites is shared by the majority of researchers [4–9]. Granite intrusions are considered to be the source of major elements necessary for the generation of rare-metal pegmatites, which suggests that rare elements accumulated either in the volatile-enriched residual melt or in the fluid-hydrothermal residue at a late stage of granite magma crystallization, while a single injection or multiple injections of magmatogenic residues and their crystallization in the surrounding rocks gave rise to the whole range of granite pegmatites. Consequently, for studying rare-metal pegmatites, it seems essential to identify their genetic relationships with granites and to determine the age of mineralization. These issues can be solved using an isotope-geochronological research aimed at the establishment of the timing for parental granites and proper pegmatites. The northeastern part of the Fennoscandian Shield (Kola Peninsula) occupies the Archaean Kolmozero–Voronya greenstone belt which accommodates fields of LCT-type rare-metal pegmatites [10]. The rare-metal pegmatites of the Kolmozero deposit have recently been subjected to careful examination due to a dramatically increased demand for lithium as a main metal for electric batteries. There are several mineralogical and geochemical types of pegmatites within the Kolmozero deposit, including feldspar, muscovite-feldspar, and albite-spodumene pegmatites [11–15]. The study of the mineral chemistry of columbite–tantalite from spodumene pegmatites of the Kolmozero deposit has made it possible to infer that the evolution of the Kolmozero pegmatites involved the following two stages: an early magmatic crystallization stage and a late hydrothermal-metasomatic stage [16]. Until now, there has been no widely accepted viewpoint concerning the genetic affinity of these pegmatites. Various authors have assumed their relationships with different types of granitoids found in the region, for example, plagiogranites and tonalites [17], amphibole-biotite granodiorites [18], microcline granites [19], and tourmaline-muscovite granites [11]. There has also been an opinion that the rare-metal pegmatites were related to granitization processes (palingenic-metasomatic granites) [20].

Of all the above points of view, a statement that tourmaline-muscovite granites are parental to spodumene pegmatites seems to be the most feasible. This is supported by a large volume of field data for the mineralogy and geochemistry of the spodumene pegmatites. There are rare-metal minerals (spodumene and lepidolite) in the pegmatoid granite schlieren and pegmatites of the exocontact zone, as well as a gradual increase of the rare-metal mineralization intensity in pegmatite veins moving away from the granite massif. According to the petrochemical research of the tourmaline-muscovite granites, it has been demonstrated that, as compared with the intermediate granites, these are significantly enriched in rare elements such as lithium, rubidium, cesium, boron, niobium, and tantalum. The concentrations of these elements increase even more in the pegmatites of the exocontact zone [11,13]. In these publications, the author identified several stages of pegmatite formation from a quartz-feldspar through to a muscovite-feldspar to an albite-spodumene stage. Albitization was followed by lithium metasomatism associated with ingress of the bulk of main rare elements such as lithium, tantalum, niobium, beryllium, and partly cesium to pegmatitic cavities [11].

The isotope data have recently been obtained for a series of rock units which could be possible candidates as parental granites for the rare-metal pegmatites of the Kolmozero–Voronya greenstone belt. These are the rocks of the differentiated sanukitoid Porosozero massif represented by a series of gabbrodiorite–quartz monzodiorite–granodiorite–microcline-plagioclase granite. The U-Pb (ID TIMS) zircon age for this rock series ranges within 2.73–2.68 Ga [21]. The plagiogranites and tonalites in the Murmansk block framing the Kolmozero–Voronya greenstone belt yields an age of 2.9–2.7 Ga [22]. The age of the alkaline-granite massifs located within the Keivy block is 2.67–2.65 Ga [23]. The U-Pb method on monazite and the Rb-Sr isochrone method on whole-rock samples have enabled researchers to estimate the age of the Kolmozero–Voronya pegmatites to be 2.7–2.6 Ga [24].

## 2. Geological Setting of the Kolmozero–Voronya Greenstone Belt

The Kolmozero–Voronya greenstone belt is confined to the central part of the suture zone separating the Murmansk block from the Central Kola and Keivy blocks. It is composed of metamorphosed and deformed volcano-sedimentary rocks by ultramafic to felsic intrusions with various

ages. The supracrustal Kolmozero–Voronya complex includes four suites such as Lyavozero (lower terrigenous unit), Polmostundra (komatiite-tholeiite series), Voron'ya tundra (basalt-andesite-dacite series), and Chervurt (upper terrigenous unit) [25]. The belt is represented by late Archaean volcano-sedimentary rocks (3.1–2.9 Ga). It concentrates rare-metal pegmatite deposits (Li and Cs with minor Nb, Ta, and Be). The northwestern part of the belt encompasses lithium and caesium deposits called Vasin Mylk, Okhmylk, Oleniy ridge, and Polmos; in its southeastern part there is the largest Kolmozero spodumene pegmatite deposit (Figure 1) [26]. Pegmatite fields of the northwestern deposits occur among Archaean amphibolites of the Polmostundra suite. The U-Pb (TIMS) microlite age was determined for the Vasin Myl'k rare-metal pegmatite deposit to be 2454 ± 8 Ma [27,28]. There are still no reliable isotope-geochronological data for the pegmatites of the Kolmozero deposit. The Kolmozero spodumene pegmatites penetrate an intrusive gabbro-anorthosite body of the Patchemvarek massif. Mesoarchaean gabbro-anorthosites occupy the border between the Murmansk block of plagiogranites and the Kolmozero–Voronya greenstone belt. The U-Pb age for a magmatic zircon from the gabbro-anorthosites of this massif is 2925 ± 7 Ma [29]. According to Vrevsky [30], the time of the massif's crystallization was estimated at 2.67 Ga, while the 2.93 Ga zircon has a xenogenic nature.
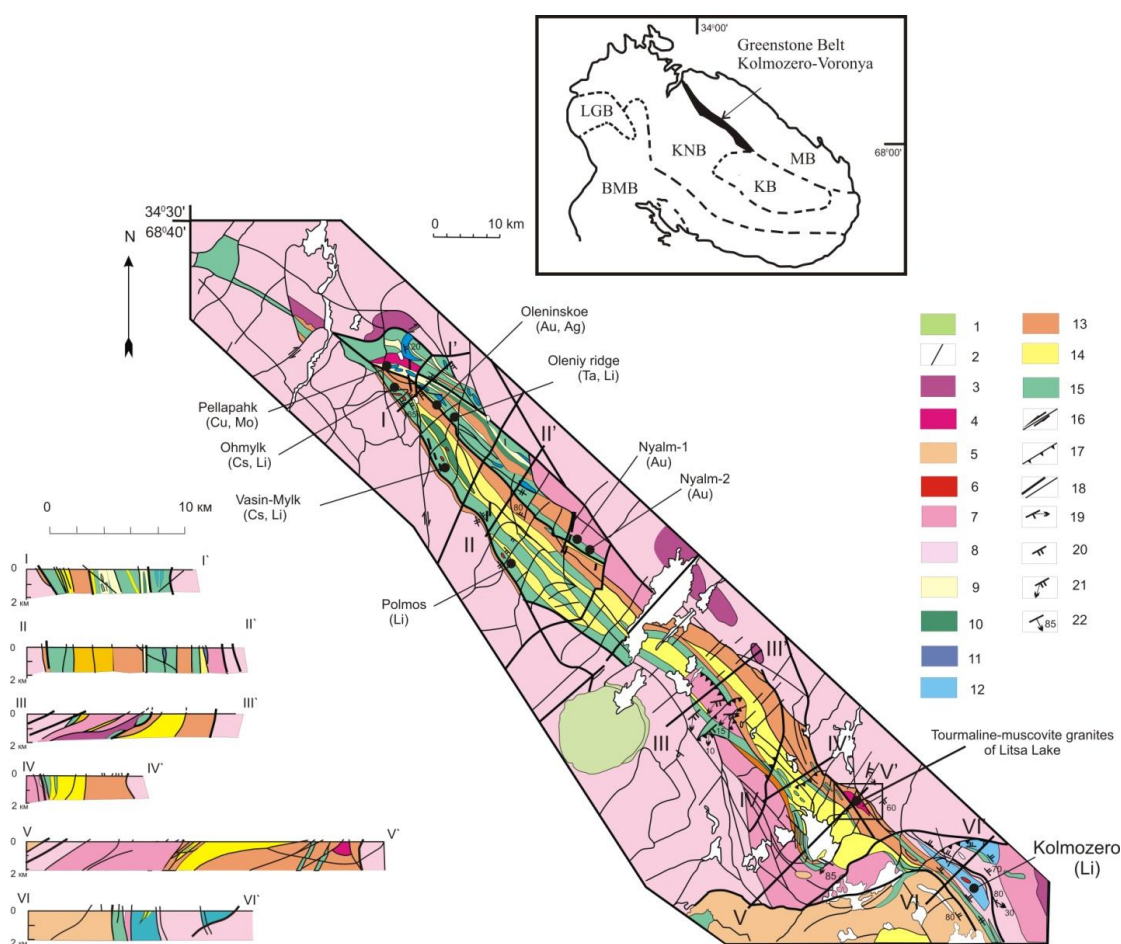


**Figure 1.** The sketch map of the Kolmozero–Voronya greenstone belt [26]. (**1**) Kontozero sedimentary-volcanogenic complex. Intrusive complexes: (**2**) Dykes of diabases and picritic porphyrites of conditionally Proterozoic age; (**3**) Microcline leucogranites; (**4**) Tourmaline granites; (**5**) Alkaline granites and metasomites on them; (**6**) Granite pegmatites with rare metal mineralization; (**7**) Quartz monzodiorites and quartz diorites; (**8**) Plagiomicrocline granites and granite-migmatites; (**9**) Quartz porphyry; (**10**) Metagabbro and gabbro-amphibolites; (**11**) Metaperidotites, metapyroxenites, actinoliths,

tremolithites; (**12**) Meta-gabbro-labradorites, amphibolites, and chlorite schists on them. Volcanic-sedimentary complexes: (**13**) Garnet-biotite and biotite gneisses, garnet-kyanite (andalusite)-biotite, garnet-kyanite-staurolite schists of the gneiss-shale complex; (**14**) Amphibole-biotite, biotite, muscovite-biotite gneisses and schists of the leptite complex (gneisses of the Lebyazhynskaya formation are marked the same color); (**15**) Amphibolites with relics of ultrabasic (komatiite) and basic metavolcanic rocks, pillow lavas, ferruginous quartzites. Structural elements: (**16**) Shifts; (**17**) Thrusts; (**18**) Tectonic disturbances of various degrees; (**19**) Cleavage with linearity; (**20**) Metamorphic banding; (**21**) Crystallization schistosity with linearity; (**22**) Layering. The inset map shows the location of the Kolmozero–Voronya greenstone belt between the Murmansk Block (MB), Kola-Norvegian Block (KNB), Keivy Block (KB), Lapland-Granulite Block (LGB), and Belomorian Mobile Belt. (BMP).

## 3. Geological Setting and Mineral Composition of the Tourmaline-Muscovite Granites (TMG)

The largest tourmaline-muscovite granite body occurs in the vicinity of Lake Litsa which is 20 km away from the Kolmozero spodumene pegmatite deposit, described in detail in [11]. The massif represents an oval-shaped stock with a length of 3.5 km and a width of ca. 1.5 km (Figure 2). It is located at the border between fine-grained biotite and garnet-biotite gneisses, staurolite-garnet-biotite gneisses and feldspar amphibolites that represent sequences of the volcano-sedimentary rock unit within the Kolmozero–Voronya belt. The massif is divided into three blocks by nearly north–south faults. The northeastern and southeastern contacts are cutting. The southwestern part of the massif exposes a xenolith of the country rock composed of amphibolites and fine-grained biotite gneisses. The amphibolites are garnetized at the contact with the granites, whereas the biotite gneisses are subject to slight muscovitization and silicification. There are two rock varieties within the massif with predominant fine-grained gneissic tourmaline-muscovite granites (with a grain size varying within 0.05–0.25 mm). The persistent occurrence of relic biotite in the muscovite shows that the muscovite is not a primary mineral in the rock. The tourmaline-muscovite granites are considered to be some kind of greisens after fine-grained biotite granites. Along the whole southern and southeastern margin of the massif near the contact with the country rocks, there is a pegmatoid granite facies. The granites of this facies demonstrate a unequigranular-coarse-grained structure (with a grain size varying within 0.5–1.5 cm) and a massive texture. As compared with the gneissic tourmaline-muscovite granite, these are markedly depleted in muscovite. The pegmatoid granites are connected to fine-grained gneissic granites by gradations and frequently resemble irregular schlieren and pockets. At the contact with the country rocks, they form numerous apophyses gradually developing into typical pegmatitic bodies with a significant thickness. This transition is expressed in a gradually increasing grain size within one vein-shaped body, in an increasing degree of differentiation resulting in quartz pockets surrounded by blocky segregations of feldspars and, finally, in an increasing concentration of accessory minerals such as tourmaline, garnet, apatite, and others in a vein-shaped body as it escapes from the granite massif into the country rocks. Such apophyses are especially abundant in the southern and southeastern parts of the massif, where the surrounding gneisses concentrate a large number of individual pegmatite veins which are quite similar to the veined pegmatoid granites in terms of composition and textural-structural features.

The above data suggests that the apical part of the intrusion was exposed in the current erosional surface. The process of the intrusion emplacement was long and complicated. Granites intruded somewhat before the main folding phase; therefore, xenoliths of the host volcano-sedimentary rock unit were preserved in their initial position in the form of gentle dome-shaped folds. The massif responded as a rigid boulder to the tectonic forcing of the main folding phase, while the country rocks were still plastic and became isoclinally folded. Later, during autometasomatism, pegmatoid granites of the massif's marginal facies formed; this was accompanied by pegmatitic injections into the country rocks. The modern appearance was acquired by the tourmaline-muscovite granite massif as a result of intensive muscovitization (greisenization) of the initially biotite-enriched fine-grained granites.
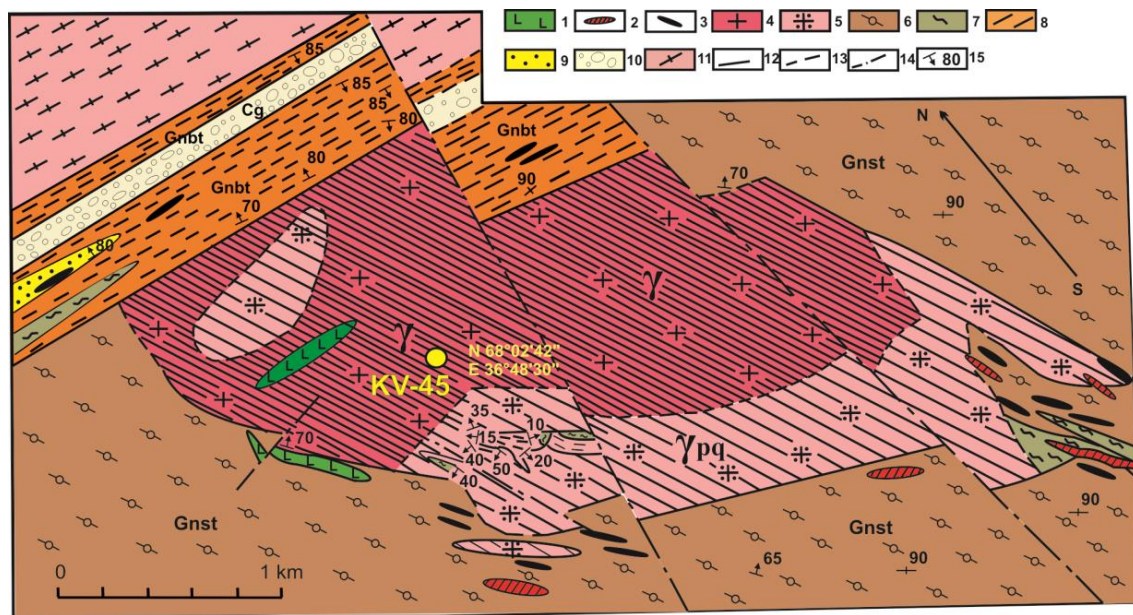
**Figure 2.** The geological map of tourmaline-muscovite granites of the Lake Litsa [11]. (**1**) Diabases; (**2**) Muscovite-feldspar pegmatites; (**3**) Feldspar pegmatites; (**4**) Fine-grained tourmaline-muscovite granites; (**5**) Coarse-grained pegmatoid rocks; (**6**) Staurolite-garnet-biotite gneisses; (**7**) Feldspar amphibolites; (**8**) Garnet-biotite gneisses; (**9**) Quartzite; (**10**) Basal conglomerates; (**11**) Oligoclase gneiss granites; (**12**) Defined geological boundaries; (**13**) Estimated geological boundaries; (**14**) Tectonic displacements; (**15**) Dips and strikes.

The tourmaline-muscovite granites represent fine-grained light-colored gneissic rocks with a lepidogranoblastic texture which becomes granoblastic or blastograntic in the areas depleted in muscovite. The main rock-forming minerals include quartz (30–40%), albite-oligoclase series plagioclase (No. 6–12, 20–30%), potassium feldspar (15–30%), and muscovite (5–15%). The minor minerals are represented by biotite (0.5–5%), tourmaline (0.5–2%), apatite (0.1–2%), and garnet (0.1–0.5%). In addition, there may be magnetite, zircon, staurolite, aegirine, hornblende, kyanite, molybdenite, pyrite, arsenopyrite, and columbite. The pegmatoid granites composing the massif's marginal part are compositionally similar to gneissic tourmaline-muscovite granites. The main rock-forming minerals involve quartz (25–35%), plagioclase (No. 5–10, 25–40%), microcline (25–40%), and muscovite (2–5%). The minor minerals are represented by tourmaline (0.5–1%), apatite (0.1–0.2%), and garnet (0.1–0.5%). The accessory minerals (below 0.1%) are found to be magnetite, ilmenite, zircon, pyrite, arsenopyrite, columbite-tantalite, and beryl [11].

## 4. Analytical Methods

Major element concentrations (reported as oxides in (Table 1) were determined by the traditional wet chemical analysis following procedures described in [31] at the Geological Institute of the Kola Science Center, RAS (Apatity). Inductively coupled plasma mass spectrometry (ICP-MS) was conducted at the Institute of Geology and Geochemistry, Ural Branch of RAS (Yekaterinburg) to obtain trace elements content (Table 1), following procedures published in [32]. The U-Pb dating and trace element analysis of zircon using secondary ion mass spectrometry (SIMS) were performed on a SHRIMP-RG ion microprobe jointly operated by Stanford University and the U.S. Geological Survey, following procedures outlined by [33] and [34]. Cathodoluminescence images of zircons were taken using a JEOL LV 5600 scanning electron microscope. Processing of the analytical data was performed using the SQUID-2 program [35]. The accuracy of U-Pb ages was checked by comparing the measurement of the in-house trace element reference material MAD-559 relative to the accepted age [34]. The weighted mean 206Pb/238U date for MAD-559 in this study yielded 521.6 ± 3.6 Ma (2σ, n = 4, MSWD = 1.42), which was

consistent with previously published ages for this internal reference material [34]. The long-term reproducibility of the trace element analyses for MAD-559 has been demonstrated in previous studies (e.g., [34]). To construct rare earth element (REE) distribution spectra, the composition of zircon was normalized for that of chondrite CI [36]. Zircon crystallization temperature was estimated using the Ti-in-Zrn thermometer [37]. When plotting U-Pb concordia diagrams, the program ISOPLOT/Ex was used [38].

**Table 1.** The whole-rock major and trace element compositions of tourmaline-muscovite granite from the Lake Litsa. n.a., element was not analyzed.

| Element | KV-45 | KV-45/1 | KV-110/1 | KV-110/2 | KV-110/3 | Tourmaline-Muscovite Granite (n = 18), [13] |
|---|---|---|---|---|---|---|
| $SiO_2$ | 74.52 | 73.14 | 73.6 | 74.21 | 75.35 | 73.83 |
| $TiO_2$ | 0.08 | 0.06 | 0.04 | 0.02 | 0.02 | 0.1 |
| $Al_2O_3$ | 14.48 | 14.78 | 14.92 | 13.78 | 13.9 | 14.22 |
| $Fe_2O_3$ | 0.62 | 0.29 | 0.05 | 0.09 | 0.13 | 0.56 |
| FeO | 0.23 | 1.12 | 1.59 | 1.56 | 1.39 | 1 |
| MnO | 0.02 | 0.07 | 0.075 | 0.18 | 0.1 | 0.058 |
| MgO | 0.14 | 0.13 | 0.12 | 0.1 | 0.1 | 0.27 |
| CaO | 0.53 | 0.62 | 0.48 | 0.29 | 0.34 | 0.8 |
| $Na_2O$ | 3.58 | 3.46 | 4.11 | 3.55 | 4.51 | 3.89 |
| $K_2O$ | 3.86 | 4.98 | 3.46 | 4.51 | 3.9 | 4.08 |
| $H_2O$ | 0.48 | 0.07 | 0.14 | 0.15 | 0.1 | 0.61 |
| $P_2O_5$ | 0.14 | 0.33 | 0.08 | 0.11 | 0.82 | 0.17 |
| S | 0.02 | 0.04 | 0.05 | 0.05 | 0.03 | n.a. |
| LOI | 1.16 | 0.61 | 0.74 | 0.54 | 0.36 | n.a. |
| Total | 99.86 | 99.7 | 99.46 | 99.14 | 101.05 | 99.59 |
| $Na_2O + K_2O$ | 7.44 | 8.44 | 7.57 | 8.06 | 8.41 | 7.97 |
| (Na + K)/Al | 0.696 | 0.751 | 0.705 | 0.779 | 0.838 | 0.761 |
| Li | 107.5 | 103.5 | 82.2 | 76.2 | 104.6 | n.a. |
| Be | 3.0 | 3.5 | 4.2 | 4.3 | 4.0 | n.a. |
| Sc | 10.3 | 5.8 | 22.2 | 18.4 | 15.1 | n.a. |
| Ti | 407.8 | 199.7 | 270.2 | 201.0 | 162.6 | n.a. |
| V | 0.78 | 0.55 | 2.16 | 1.73 | 1.75 | n.a. |
| Cr | 261.5 | 131.8 | 683.9 | 601.9 | 580.8 | n.a. |
| Mn | 261 | 889 | 988 | 2685 | 1449 | n.a. |
| Co | 0.68 | 1.67 | 2.30 | 2.37 | 2.28 | n.a. |
| Ni | 2.06 | 31.0 | 33.0 | 30.4 | 38.3 | n.a. |
| Cu | 4.17 | 8.46 | 15.43 | 14.74 | 14.10 | n.a. |
| Zn | 27.5 | 25.4 | 26.2 | 34.5 | 30.2 | n.a. |
| Ga | 30.7 | 31.6 | 44.5 | 42.1 | 36.3 | n.a. |
| Ge | 2.16 | 3.66 | 2.86 | 3.53 | 3.28 | n.a. |
| As | 1.83 | 1.44 | 3.00 | 5.63 | 5.47 | n.a. |
| Se | 0.35 | 0.41 | 0.49 | 0.63 | 0.44 | n.a. |
| Rb | 264.4 | 352.2 | 436.9 | 716.2 | 585.2 | n.a. |
| Sr | 15.7 | 16.2 | 10.9 | 6.7 | 6.5 | n.a. |
| Y | 7.5 | 4.6 | 22.2 | 26.7 | 12.6 | n.a. |
| Zr | 19.6 | 15.2 | 19.2 | 25.3 | 20.2 | n.a. |
| Nb | 14.1 | 16.4 | 35.3 | 29.0 | 14.1 | n.a. |
| Mo | 0.08 | 1.09 | 2.58 | 2.11 | 2.43 | n.a. |
| Ag | 0.61 | 0.49 | 0.97 | 0.92 | 0.48 | n.a. |
| Cd | 0.08 | 0.13 | 0.10 | 0.13 | 0.08 | n.a. |
| Sn | 6.22 | 5.04 | 17.26 | 10.64 | 4.38 | n.a. |
| Sb | 0.03 | 0.06 | 0.16 | 0.16 | 0.17 | n.a. |
| Te | n.a | n.a | n.a | n.a | n.a | n.a. |
| Cs | 10.4 | 8.6 | 10.1 | 22.7 | 17.9 | n.a. |
| Ba | 15.8 | 14.4 | 16.2 | 17.7 | 12.0 | n.a. |

**Table 1.** *Cont.*

| Element | KV-45 | KV-45/1 | KV-110/1 | KV-110/2 | KV-110/3 | Tourmaline-Muscovite Granite (n = 18), [14] |
|---|---|---|---|---|---|---|
| La | 2.8 | 0.77 | 6.42 | 6.88 | 3.32 | n.a. |
| Ce | 6.3 | 1.9 | 14.9 | 15.0 | 8.2 | n.a. |
| Pr | 0.74 | 0.23 | 1.86 | 1.83 | 0.99 | n.a. |
| Nd | 2.53 | 0.80 | 6.44 | 6.59 | 3.47 | n.a. |
| Sm | 0.95 | 0.46 | 2.75 | 2.88 | 1.44 | n.a. |
| Eu | 0.053 | 0.049 | 0.042 | 0.033 | 0.019 | n.a. |
| Gd | 1.12 | 0.59 | 2.97 | 3.33 | 1.53 | n.a. |
| Tb | 0.21 | 0.13 | 0.54 | 0.59 | 0.27 | n.a. |
| Dy | 1.16 | 0.69 | 2.92 | 3.35 | 1.60 | n.a. |
| Ho | 0.18 | 0.10 | 0.44 | 0.54 | 0.26 | n.a. |
| Er | 0.46 | 0.29 | 1.28 | 1.57 | 0.77 | n.a. |
| Tm | 0.07 | 0.05 | 0.20 | 0.26 | 0.13 | n.a. |
| Yb | 0.44 | 0.37 | 1.50 | 1.99 | 1.04 | n.a. |
| Lu | 0.06 | 0.05 | 0.18 | 0.28 | 0.14 | n.a. |
| Hf | 0.74 | 0.81 | 0.95 | 1.40 | 1.27 | n.a. |
| Ta | 1.66 | 3.04 | 3.51 | 2.90 | 2.09 | n.a. |
| W | 1.79 | 1.65 | 3.89 | 2.42 | 1.33 | n.a |
| Tl | 0.82 | 1.17 | 1.11 | 2.01 | 1.77 | n.a. |
| Pb | 10.3 | 18.1 | 13.1 | 13.2 | 11.5 | n.a. |
| Bi | 5.24 | 2.29 | 0.35 | 0.88 | 0.90 | n.a. |
| Th | 2.03 | 0.43 | 11.8 | 13.9 | 5.6 | n.a. |
| U | 5.87 | 3.90 | 9.01 | 25.9 | 11.4 | n.a. |

## 5. Results

### 5.1. Major and Trace Element Composition of Tourmaline-Muscovite Granites (TMG)

Almost all the rocks studied (Table 1) are characterized by relatively high alkalinity. For the rocks of tourmaline-muscovite granites (TMG) with $SiO_2$ content from 73.14 to 75.35 wt.%, the $Na_2O$ + $K_2O$ sum varies within 7.44–8.44 wt.%, and an agpaitic index (molar proportion of (Na + K)/Al) amounts to 0.70−0.84. According to the petrochemical classification [39], these are subalkaline granites (Figure 3). The TMG show the following major-element geochemical characteristics: The $SiO_2$ contents range from 73.14 to 75.35 wt.%, $Al_2O_3$ from 13.78 to 14.92 wt.%, CaO from 0.29 to 0.85 wt.%, $Na_2O$ from 3.46 to 4.51 wt.%, and $K_2O$ from 3.49 to 4.98 wt.% (Table 1). The results of whole-rock trace element analyses are listed in Table 1. Chondrite-normalized REE plots demonstrate (Figure 4) the enrichment of LREE as compared with HREE ($La_N/Yb_N$ 1.4–4.3) and an Eu anomaly ($Eu_N/Eu_N$* 0.02–0.14). The TMG are enriched in large ion lithophile elements (LILE) and virtually depleted in high field strength elements (HFSE). The TMG are characterized by the following contents of rare earth elements (total REE = 7–45 ppm): Li 76–108 ppm, Rb 264–716 ppm, Cs 9–23 ppm, Y 4–27 ppm, Ta 1.7–3.5 ppm, U 4–26 ppm; low concentrations of Sr 7–16 ppm, Zr 15–25 ppm, Ba 12–18 ppm, and Th 0.4–13.9 ppm (Figure 5).
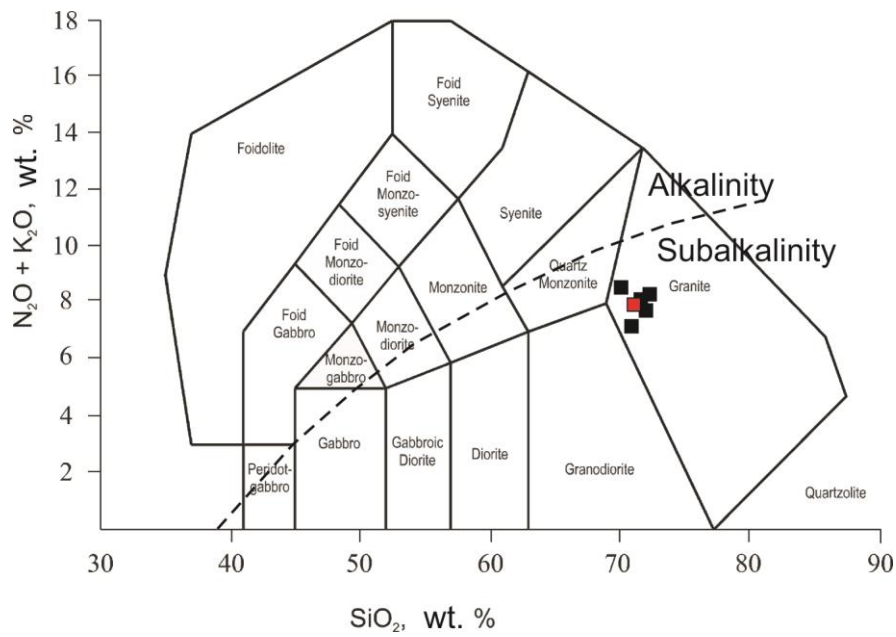
**Figure 3.** The classification diagram $SiO_2$-$Na_2O + K_2O$ for tourmaline-muscovite granite of the Lake Litsa (data sources from Table 1) [39]. The red box marks the mean of 18 samples from tourmaline-muscovite granite [13].
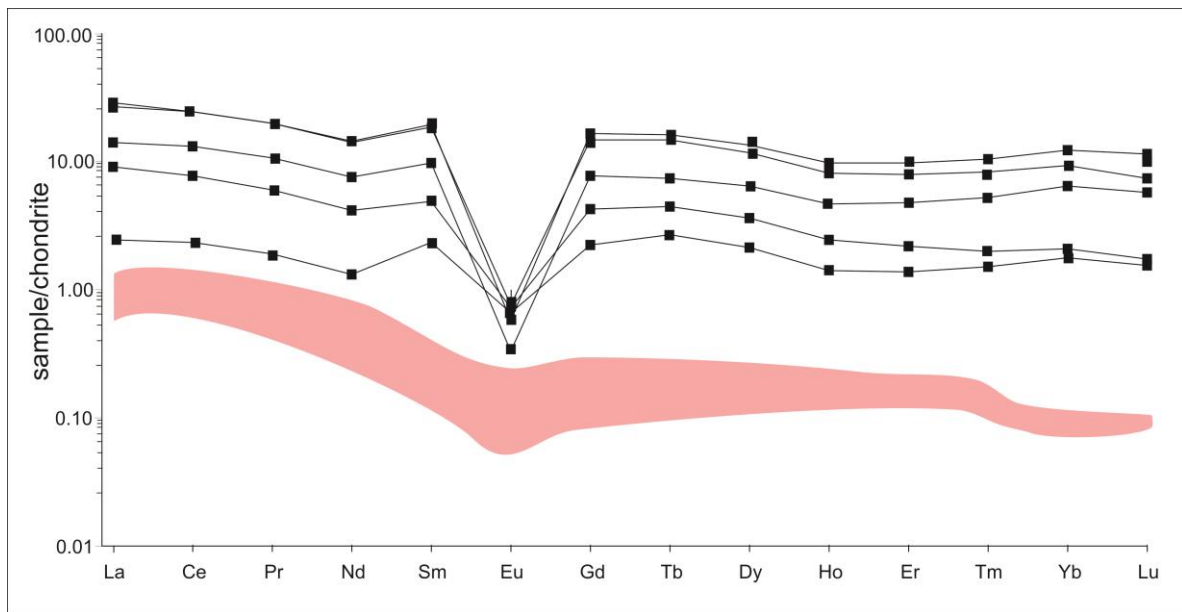


**Figure 4.** Chondrite-normalized rare earth element (REE) diagrams for the studied tourmaline-muscovite granites (TMG) (data sources from Table 1) as compared with the pegmatite of the Kolmozero deposit (pink field) (see [15] for data sources). Normalizing chondrite values [36].
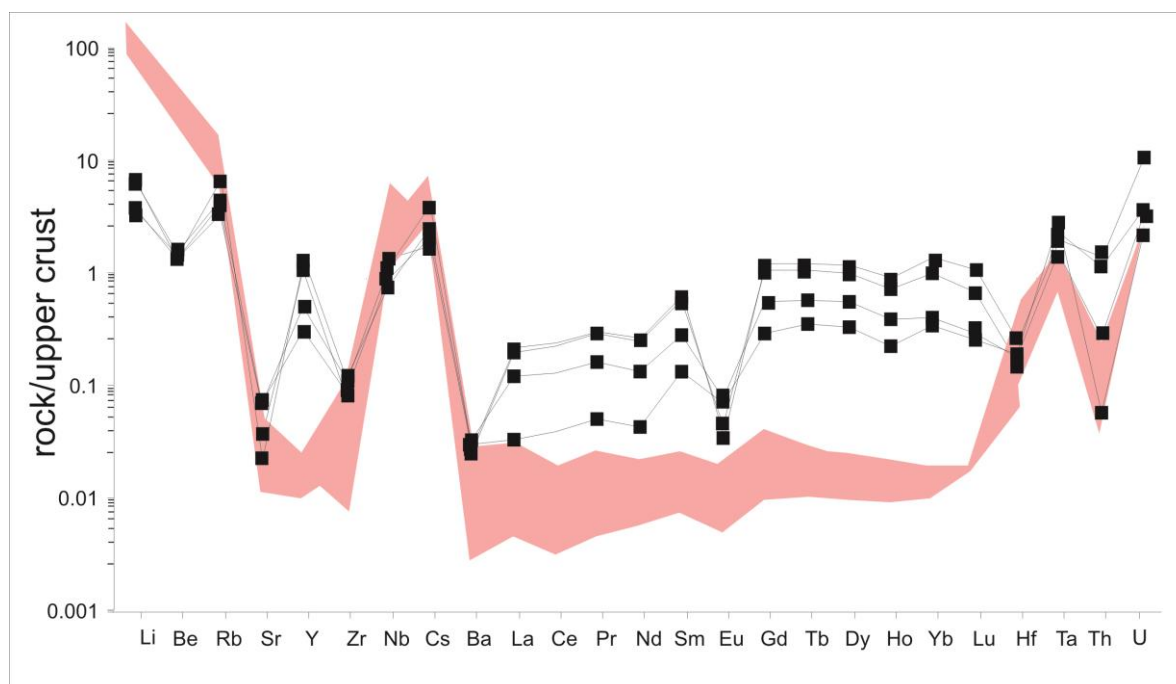
**Figure 5.** Multi-element spider diagrams normalized to Upper Crust composition [40] for the studied TMG as compared with the pegmatite of the Kolmozero deposit (pink field) (see [15] for data sources).

*5.2. SIMS (REE) Study of Zircons*

In general, the distribution spectra are similar to each other and flatten out in the field of light REE ($Sm_N/La_N$ ratio ranges from 1.86 to 9.63 at point 4.1–78.2) (Table 2). The total REE concentration at the zircon rims varies from 287 to 6824 ppm, averaging 2774 ppm. The total REE concentration in the zircon cores varies from 340 to 2840 ppm, averaging 980 ppm (Table 2). Light REE concentrations at the zircon rims range from 43 to 2052 ppm (averaging 492 ppm) and from 15 to 709 (averaging 202 ppm) in the zircon cores. Heavy REE content at the zircon rims varies from 244 to 4771 ppm, averaging 1847 ppm, and from 325 to 2132 ppm, averaging 778 ppm, in the zircon cores. Zircon from the TMG shows a poor light-to-heavy REE differentiated pattern ($Yb_N/La_N$ ratio averages 1502) in the diagram for REE spectra (Figure 6). A positive Ce-anomaly is poorly defined (Ce/Ce* averages 2.36 and, at point 4.1, Ce/Ce* = 82.5) (Table 2). All points demonstrate a slight positive Eu-anomaly Eu/Eu* varying from 0.08 to 1.17, averaging 0.29 (Table 2).

By examining the features of the rare and rare earth element distribution patterns, the zircons from the TMG are attributed to a metasomatic type. In the diagram that correlates the light REE differentiation degree and a Ce anomaly value [41], nine points of zircons lie in the field of hydrothermal-metasomatic varieties or nearby (Figure 7). Only the point 4.1 falls in the field of igneous zircons (Figure 7). In the altered zircons, the Ti content averages 295 ppm, being ca. 16 ppm in less altered varieties. Consequently, the zircon crystallization temperatures calculated using a Ti thermometer [37] should be treated with caution. Accordingly, it is most reasonable to apply temperatures only for the less altered areas of zircons. Such a temperature interval has been evaluated to be 650–850 °C (Table 2).

**Table 2.** Trace element concentrations (ppm) in zircons from the tourmaline-muscovite granites of the Lake Litsa.

| Spot | Grain 1 | | Grain 2 | | Grain 3 | Grain 4 | | Grain 5 | | Grain 6 |
|---|---|---|---|---|---|---|---|---|---|---|
| Elements | 1.1 | 1.2 | 2.1 | 2.2 | 3.1 | 4.1 | 4.2 | 5.1 | 5.2 | 6.1 |
| Ti | 20.8 | 188.7 | 439.9 | 41.9 | 20.8 | 2.4 | 111.5 | 28.5 | 13.3 | 4.7 |
| Fe | 661 | 2266 | 3666 | 497 | 154 | 36 | 5117 | 116 | 204 | 433 |
| Y | 1311 | 5057 | 2192 | 582 | 384 | 452 | 3243 | 622 | 438 | 605 |
| La | 34.75 | 108.92 | 61.36 | 39.53 | 7.02 | 0.02 | 121.01 | 5.90 | 3.16 | 3.71 |
| Ce | 143 | 751 | 306 | 134 | 48 | 13 | 569 | 35 | 19 | 24 |
| Nd | 37.7 | 407.7 | 142.3 | 57.4 | 18.1 | 0.4 | 333.7 | 11.5 | 8.9 | 4.0 |
| Sm | 52.9 | 659.5 | 190.5 | 56.0 | 31.4 | 0.9 | 273 | 18.1 | 11.4 | 4.3 |
| Eu | 6.69 | 125.34 | 8.92 | 5.72 | 1.93 | 0.27 | 20.74 | 1.18 | 0.48 | 0.27 |
| Gd | 161 | 2194 | 571 | 139 | 91 | 8 | 529 | 80 | 52 | 18 |
| Dy | 247 | 1265 | 580 | 139 | 100 | 40 | 615 | 136 | 91 | 67 |
| Er | 204 | 506 | 246 | 68 | 47 | 86 | 358 | 79 | 49 | 113 |
| Yb | 448 | 807 | 734 | 102 | 110 | 191 | 426 | 97 | 52 | 211 |
| Hf | 11,798 | 15,586 | 24,748 | 10,207 | 12,776 | 10,386 | 14,073 | 9667 | 12,135 | 12,371 |
| Th/U | 0.31 | 0.08 | 0.03 | 0.03 | 0.03 | 0.44 | 0.07 | 0.14 | 0.08 | 0.09 |
| Eu/Eu* | 0.22 | 0.32 | 0.08 | 0.20 | 0.11 | 0.30 | 1.17 | 0.09 | 0.06 | 0.09 |
| Ce/Ce* | 2.11 | 1.90 | 1.75 | 1.50 | 2.29 | 82.55 | 1.51 | 2.25 | 1.93 | 3.41 |
| $\Sigma REE$ | 1336.60 | 6823.97 | 2840.76 | 740.26 | 454.04 | 340.55 | 3246.13 | 463.16 | 287.48 | 445.35 |
| $\Sigma LREE$ | 275.45 | 2052.49 | 708.78 | 292.69 | 106.64 | 15.08 | 1317.74 | 71.49 | 43.19 | 36.70 |
| $\Sigma HREE$ | 1061.15 | 4771.48 | 2131.98 | 447.58 | 347.39 | 325.47 | 1928.40 | 391.67 | 244.29 | 408.64 |
| $Yb_n/La_n$ | 19.12 | 10.99 | 17.74 | 3.82 | 23.23 | 14809.1 | 5.22 | 24.40 | 24.41 | 84.31 |
| $Sm_n/La_n$ | 2.42 | 9.63 | 4.94 | 2.25 | 7.10 | 78.22 | 3.59 | 4.89 | 5.75 | 1.86 |
| T(Ti), C° | 859 | 1189 | 1373 | 946 | 858 | 654 | 1093 | 896 | 809 | 709 |
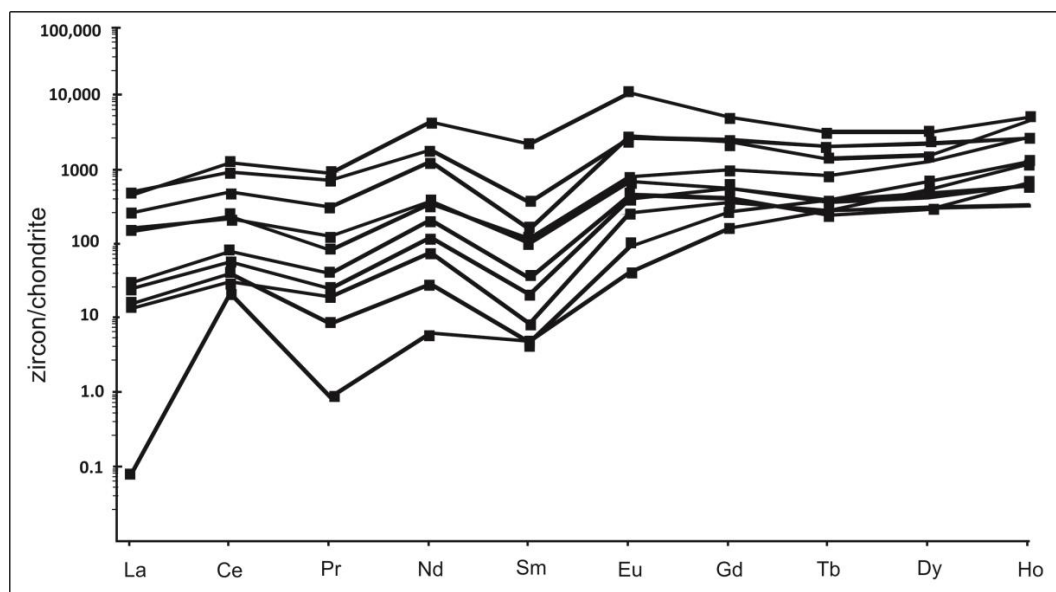


**Figure 6.** Chondrite-normalized REE patterns for zircon from TMGs (data sources from Table 2). Normalizing chondrite values [36].
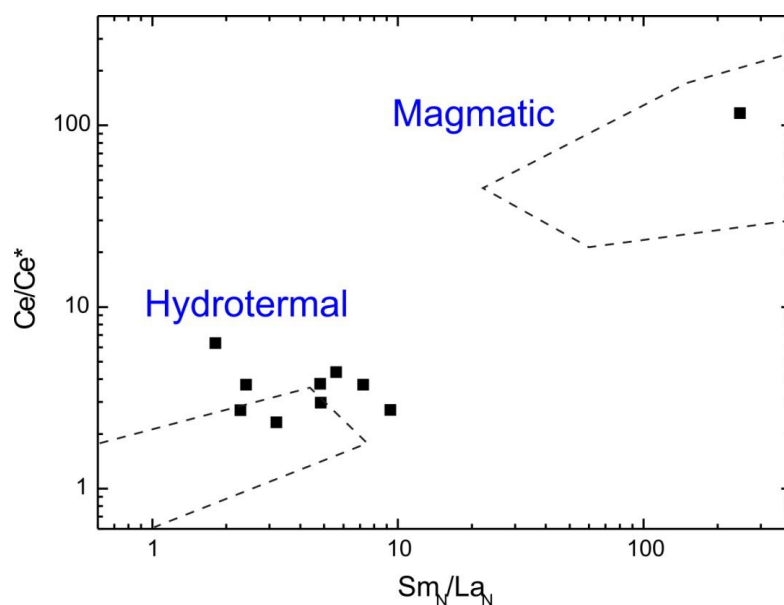
**Figure 7.** The ratio between the degree of the fractionation of LREE ($Sm_N/La_N$) and the value of the Ce anomaly (Ce/Ce*) (data sources from Table 2). Fields of magmatic and hydrothermal-metasomatic zircons are given after [41].

### 5.3. U-Pb (SHRIMP RG) Dating of Zircons

Zircon from sample (KV-45) was separated from the central part of the tourmaline-muscovite granite massif (Figure 2). Grains are represented by altered brown zircon-type crystals with a grain size of 100–200 μm. In cathodoluminescence, zircon shows phase heterogeneity with lighter semi-transparent cores and dark and opaque margins. In the centers of some analyzed grains, there are areas with thin euhedral growth zoning (Figure 8).
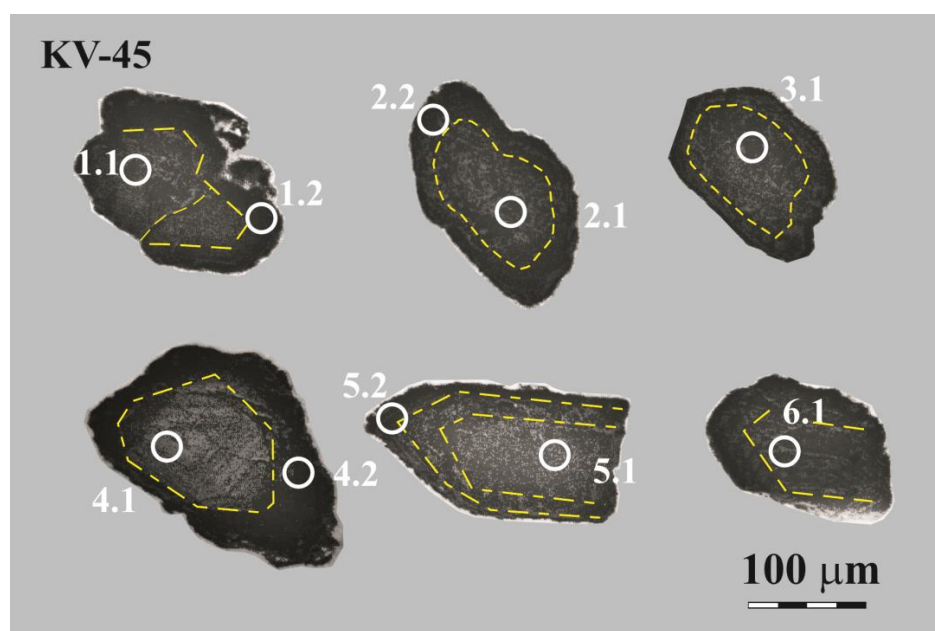


**Figure 8.** Cathodoluminescence images of zircon grains from the tourmaline-muscovite granite. White circles indicate the analytical spots. Yellow dashed lines indicate the boundaries between light and dark areas of zircon.

Two discordia were plotted for 10 analyzed zircon points; one discordia on four analyzed points lying on the rims of the grains (points 1.2, 2.2, 4.2, and 5.2) and the other on five points located in the central parts of the crystals (points 1.1, 2.1, 4.1, 5.1, and 6.1) (Figure 8). A discordant age of 2728 ± 14 Ma, MSWD = 0.70, is obtained for four points from the marginal parts. Point 4.1 with a rare earth element distribution spectrum typical of an igneous zircon occurs near the concordia (D = +3%) and its $^{207}$Pb/$^{206}$Pb age is 2794 ± 7 Ma (Table 3).

A discordant age of 2802 ± 13 Ma, MSWD = 0.89, is obtained for five points from the zircon cores (Figure 8). The isotope $^{207}$Pb/$^{206}$Pb age of analytical point 3.1 was found to be 2909 ± 7 Ma and was ignored. Figure 9 shows that the analytical points are strongly discordant and indicative of the disturbance of the U-Pb system due to the removal of lead. Zircon in the marginal parts is enriched in uranium at 950–2500 ppm and has a low U/Th ratio of 0.03:0.08. The zircon cores reveal a lower uranium content, 173–1712 ppm, at a significantly higher U/Th ratio of 0.14:0.45. Thus, the upper discordia and concordia intersection with an age of 2802 ± 13 Ma most probably reflects the time of zircon crystallization during the formation of the tourmaline-muscovite granites, whereas the age of 2728 ± 14 Ma yields the time of a hydrothermal-metasomatic process. More ancient values for the zircon age (point 3.1, $^{207}$Pb/$^{206}$Pb = 2909 ± 7 Ma) could apparently suggest the availability of an ancient lead component preserved in some areas of zircon grains.
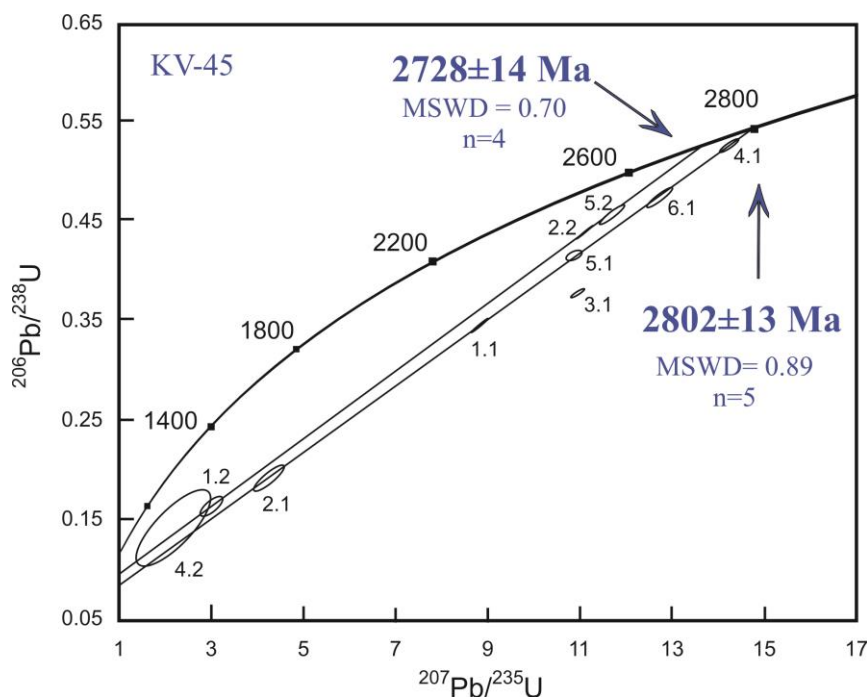


**Figure 9.** U-Pb Concordia diagram of SHRIMP-RG analyses for the zircon from the tourmaline-muscovite granite (data from Table 3).

**Table 3.** Results of U-Pb dating of zircons (sample KV45).

| Grain | $^{206}Pb_c$, % | Content, ppm | | | $^{232}Th/^{238}U$ | Corrected rations ± % (1s) | | | RhO | Age ± 1s, Ma | | D, % |
|---|---|---|---|---|---|---|---|---|---|---|---|---|
| | | $^{206}Pb*$ | U | Th | | $^{207}Pb/^{206}Pb$ | $^{207}Pb/^{235}U$ | $^{206}Pb/^{238}U$ | | $^{206}Pb/^{238}U$ | $^{207}Pb/^{206}Pb$ | |
| KV-45-4.2 | 0.191 | 406 | 3308 | 225 | 0.07 | 0.111 ± 16.0 | 2.19 ± 24.0 | 0.143 ± 18.4 | 0.8 | 861 ± 149 | 1814 ± 290 | +56 |
| KV-45-1.2 | 0.052 | 350 | 2776 | 226 | 0.08 | 0.148 ± 3.9 | 2.98 ± 5.7 | 0.161 ± 4.2 | 0.7 | 882 ± 34 | 2318 ± 66 | +66 |
| KV-45-2.1 | 0.075 | 277 | 1712 | 42 | 0.03 | 0.162 ± 2.3 | 4.21 ± 5.2 | 0.189 ± 4.7 | 0.9 | 1114 ± 48 | 2477 ± 38 | +60 |
| KV-45-2.2 | 0.032 | 262 | 693 | 20 | 0.03 | 0.183 ± 0.2 | 11.10 ± 0.9 | 0.439 ± 0.9 | 1.0 | 2347 ± 18 | 2683 ± 4 | +15 |
| KV-45-5.1 | 0.000 | 150 | 422 | 59 | 0.14 | 0.184 ± 0.8 | 10.84 ± 1.1 | 0.415 ± 0.7 | 0.7 | 2237 ± 14 | 2693 ± 13 | +20 |
| KV-45-1.1 | 0.023 | 290 | 979 | 301 | 0.32 | 0.185 ± 0.2 | 8.80 ± 1.3 | 0.344 ± 1.3 | 1.0 | 1908 ± 22 | 2702 ± 4 | +34 |
| KV-45-5.2 | 0.009 | 404 | 1032 | 84 | 0.08 | 0.186 ± 0.5 | 11.67 ± 1.5 | 0.456 ± 1.4 | 0.9 | 2421 ± 29 | 2704 ± 9 | +13 |
| KV-45-6.1 | 0.006 | 417 | 1030 | 96 | 0.10 | 0.196 ± 0.6 | 12.75 ± 1.5 | 0.472 ± 1.4 | 0.9 | 2491 ± 28 | 2793 ± 10 | +13 |
| KV-45-4.1 | 0.000 | 78 | 173 | 76 | 0.45 | 0.196 ± 0.4 | 14.19 ± 1.0 | 0.525 ± 0.9 | 0.9 | 2719 ± 20 | 2794 ± 7 | +3 |
| KV-45-3.1 | 0.006 | 303 | 937 | 27 | 0.03 | 0.210 ± 0.4 | 10.93 ± 0.9 | 0.377 ± 0.8 | 0.9 | 2060 ± 13 | 2909 ± 7 | +34 |

Error in the calibration standard is 0.29%; $^{206}Pbc$ and $^{206}Pb*$, common and radiogenic lead; corrected ratios and $^{206}Pb$ content are corrected for $^{204}Pbc$; D is discordance, D = 100 × (age ($^{207}Pb/^{206}Pb$)/age ($^{207}Pb/^{238}U$) − 1). Rho is the error correlation coefficient of radiogenic $^{206}Pb/238U$ vs. $^{207}Pb/^{235}U$.

## 6. Discussion

Worldwide, there are many cases where one can observe a clear transition from granites to pegmatite veins with a rare-metal mineralization [6,8,9,42–45]. Usually, these are structurally well-developed granite plutons, and their geochemical and isotope-geochronological data reliably indicate their relationship with pegmatites. However, it is frequently difficult to establish the relationship between the pegmatites and parental granites. This is caused by the fact that the pegmatitic bodies can migrate for many kilometers from the source and that the parental granites can be destroyed by the erosional processes lying above the level of the modern location of the pegmatite veins. Moreover, a long geological evolution of the Archaean structures also complicates the search for the sources of matter for the rare-metal pegmatites.

The zircon from the tourmaline-muscovite granites demonstrates a heterogeneous internal structure. It has a sinuous and uneven shape that cuts and obscures the initial growth zoning in the central zones of zircons. The availability of such structural zones means that the primary crystals are not always in equilibrium with the crystallizing medium (Figure 8). Despite the fact that zircon is stable in crustal and upper-mantle conditions, it is known that the solubility of zircon increases in the presence of water and fluids [46–49]. Experimental data show that zircon can be transformed at temperatures below 200 °C in the presence of aqueous fluids, including structural and chemical transformations accompanied by a change in CL intensities [50,51]. The mechanism for the formation of such zircons is complicated and includes several genetic processes [52]. In addition, the ability of zircon to transform increases in the minerals with a disturbed structure due to metamictness, fracturing or plastic deformation. Zircons with the highest U and Th concentrations are most vulnerable to alterations which result in heavy disturbances of the crystal structure due to the radioactive decay of those elements [53,54]. The U and Th concentrations in zircon from the TMG strongly vary demonstrating U/Th = 0.14–0.45 in the cores and U/Th = 0.03–0.08 at the rims (Table 2). A non-altered igneous zircon usually shows U/Th > 0.1 [55,56], whereas for metamorphic (or metasomatic) zircons, the U/Th ratio is typically less than 0.1 [57]. The studied zircons are similar in terms of their specific parallelism and nearly flat REE distribution (Figure 6). A slight negative Eu anomaly in metasomatic zircon spectra is probably explained by the presence of feldspars which isolate Eu [58,59]. The determination of the zircon crystallization temperature is an important factor for the evaluation of the crystallizing medium. The Ti-in-zircon thermometer is based on the principle that, in a buffered assemblage, the incorporation of Ti in zircon depends on T [60,61]. Ti-in-zircon thermometry has its limitations. Zircon from the TMG contains various Ti concentrations in certain zones. In the most altered zircon rims, the calculated temperature values exceeding 900 °C make no sense; in less altered areas, the temperature can be estimated using this thermometer in the wide range of 650–850 °C.

For all granitoids occurring within the greenstone belt, the isotope-geochronological data yield a Meso-Neoarchaean age [22]. The time of regional amphibolite-facies metamorphism for the rocks of the belt is evaluated to be Neoarchaean, i.e., within 2.77–2.73 Ga [62,63]. The rocks of the Keivy block which border with the Kolmozero–Voronya belt in the northeast (Figure 1) are composed of Archaean metasedimentary strata which are intruded by subalkaline anorogenic granites with an age of 2.67–2.65 Ga [23]. The isotope-geochronological data obtained for zircons from the TMG also indicate the Neoarchaean time of the formation and further metasomatic transformation of the zircon from the melt enriched in a fluid phase.

## 7. Conclusions

The U-Pb isotopic dating of zircons carried out for the TMG of the Kolmozero–Voronya greenstone belt is indicative of two episodes. The first episode is directly related to the crystallization of the tourmaline-muscovite granite intrusion, while the subsequent episode involves their intense hydrothermal-metasomatic processing. The central parts of the zircon from the tourmaline-muscovite granites show signs of crystallization from the melt enriched in a fluid phase. The marginal parts of the zircon predominantly indicate a deep zircon hydrothermal-metasomatic processing. Nevertheless,

it is not implausible that the resultant isotope data for all zircon grains could reflect one single episode where the fluid impact continued after crystallization having irregularly reflected in the zircon composition and correspondingly in the configuration of the REE distribution spectra which are typical of a metasomatic zircon. Similar features are observed in zircons from the gold prospects that occur in the northwestern part of the Kolmozero–Voronya greenstone belt (Figure 1) [63].

The 2802 ± 13 Ma zircon age for the tourmaline-muscovite granites that expose in the southeastern part of the belt near Lake Litsa reflects the Neoarchaean stage of the TMG formation. The main peak of the massif rock hydrothermal-metasomatic processing took place 2728 ± 14 million years ago. This process most probably resulted in the formation of granite pegmatites in the southern marginal part of the massif (Figure 2). Further differentiation of the residual granite melt caused generation of various pegmatite types, i.e., from quartz-feldspar to muscovite-feldspar and spodumene pegmatites of the Kolmozero deposit. It should be emphasized that, for a more precise attribution of the TMG as parental rocks for the spodumene pegmatites, it is necessary to undertake additional isotope-geochronological studies of mineral geochronometers (tantalite-columbite, apatite, cassiterite, etc.) extracted directly from the spodumene pegmatites. On the basis of the available isotope-geochronological data it has been concluding that the rare-metal sodium-lithium pegmatites of the Kolmozero deposit with a 2728 ± 14 Ma U-Pb age on zircon from the tourmaline-muscovite granites changed in time with the development of the lithium-caesium pegmatites (Vasin Myl'k deposit) with a 2454 ± 8 Ma U-Pb age on microlite from the pollucite pegmatites [27]. Despite the fact that all the rare-metal pegmatite deposits spatially tended to be in the same greenstone belt, the researchers distinguished two pegmatite fields, which were the northwestern one and the southeastern one separated by a large nearly east-west-trending fault in the center of the greenstone belt (Figure 1). Each field has its own rare-metal profile. The northwestern field comprises pollucite deposits with cesium and tantalum-niobium mineralization while the south-eastern field is related to the lithium ores. A long break (ca. 300 myr) in the formation of the rare-metal pegmatite deposits within these two pegmatite fields is presently hard to explain. It could be related to asynchronous granite-forming processes, each of which reflected two stages of tectonic activation. The presumably earlier (Neoarchaean) stage was linked to the processes of the ~2.7 Ga regional metamorphism [62,63]. The later (Early Proterozoic) stage is attributed to the influence of the ~2.45 Ga plume-tectonic processes, which are common within the Kola Peninsula and gave rise to layered mafic-ultramafic intrusions of that age [64,65].

**Author Contributions:** Conceptualization, N.M.K. and O.V.U.; Data curation, N.M.K.; Formal analysis, N.M.K. and E.N.S.; Investigation, N.M.K., O.V.U. and M.A.C.; Writing—original draft, N.M.K., O.V.U. and E.N.S.; Writing-original draft preparation, N.M.K.; Writing-review and editing, N.M.K.; M.A.C.; O.V.U. and E.N.S. All authors have read and agreed to the published version of the manuscript.

**Conflicts of Interest:** The authors declare no conflict of interest.

## References

1. Zagorsky, V.E.; Makagon, V.M.; Shmakin, B.M. *Granitic Pegmatites. Rare-Metal Pegmatites*; Siberian Branch of the Russian Academy of Sciences: Novosibirsk, Russia, 1997; Volume 2, pp. 1–278. (In Russian)
2. Tkachev, A.V. Evolution of metallogeny of granitic pegmatites associated with orogens throughout geological time. *Geol. Soc. London, Spéc. Publ.* **2011**, *350*, 7–23. [CrossRef]
3. Mccauley, A.; Bradley, D.C. The global age distribution of granitic pegmatites. *Can. Miner.* **2014**, *52*, 183–190. [CrossRef]
4. Černý, P. Petrogenesis of granitic pegmatites. In *Granitic Pegmatites in Science and Industry*; Mineral. Assoc. Can. Short Course; Mineralogical Association of Canada: Québec, QC, Canada, 1982; Volume 8, pp. 405–461.
5. Černý, P. Rare-element granite pegmatites. Part I: Anatomy and internal evolution of pegmatite deposits. *Geosci. Can.* **1991**, *18*, 49–67.

6. Černý, P. Rare-element granite pegmatites. Part II: Regional to global environments and petrogenesis. *Geosci. Can.* **1991**, *18*, 68–81.

7. Černý, P.; London, D.; Novak, M. Granitic pegmatites as reflections of their sources. *Elements* **2012**, *8*, 257–261. [CrossRef]

8. London, D. Pegmatites. *Can. Mineral.* **2008**, *10*, 347.

9. London, D. Ore-forming processes within granitic pegmatites. *Ore Geol. Rev.* **2018**, *101*, 349–383. [CrossRef]

10. Černý, P.; Ercit, T.S. Classification of granitic pegmatites. *Can. Miner.* **2005**, *43*, 2005–2026. [CrossRef]

11. Gordienko, V.V. *Mineralogy, Geochemistry and Genesis of Spodumene Pegmatites*; Nedra: Leningrad, Russia, 1970; 240p. (In Russian)

12. Gordienko, V.V.; Krivovichev, V.G.; Syritso, L.F. *Metasomitites of Pegmatite Fields*; LGU: Leningrad, Russia, 1987; 221p. (In Russian)

13. Gordienko, V.V. *Granite Pegmatites*; Saint Petersburg University: St. Petersburg, Russia, 1996; 272p. (In Russian)

14. Voloshin, A.V.; Pakhomovsky, Y.A. *Ta and Nb Mineralogy in Rare-Metal Pegmatites*; Nauka: Leningrad, Russia, 1988; 240p. (In Russian)

15. Morozova, L.N. Lithium Kolmozero deposit of rare metal pegmatites: New data on rare element composition (Kola peninsula). *Lithosphere* **2018**, *18*, 82–98. [CrossRef]

16. Badanina, E.V.; Sitnikova, M.A.; Gordienko, V.V.; Melcher, F.; Gabler, H.-E.; Lodziak, J.; Syritso, L.F. Mineral chemistry of columbite-tantalite from spodumene pegmatites of Kolmozero, Kola Peninsula (Russia). *Ore Geol. Rev.* **2015**, *64*, 720–735. [CrossRef]

17. Ginzburg, A.I.; Timofeev, I.N.; Pheldman, L.G. *Fundamentals of the Geology of Granite Pegmatites*; Nauka: Moscow, Russia, 1979; 296p. (In Russian)

18. Maslennikov, V.A. *Stratigraphy of the Polmos and Poros Formations*; LAGED: Leningrad, Russia, 1963; Volume 15, pp. 69–72. (In Russian)

19. Sosedko, A.F. *Materials on Geology and Geochemistry of Granite Pegmatites*; Gosgeoltekhizdat: Moscow, Russia, 1961; 152p. (In Russian)

20. Batieva, I.D.; Bel'kov, I.V.; Vetrin, V.R.; Vinogradov, A.N.; Efimov, M.M.; Belolipetskii, A.P.; Bolotov, V.I.; Vinogradova, G.V.; Dokuchaeva, V.S.; Dubrovskii, M.I.; et al. *Precambrian Igneous Formations of the Northeastern Part of the Baltic Shield*; Nauka: Leningrad, Russia, 1985; 176p. (In Russian)

21. Kudryashov, N.M.; Petrovsky, M.N.; Mokrushin, A.V.; Elizarov, D.V. Neoarchean sanukitoid magmatism in the Kola Region: Geological, petrochemical, geochronological, and isotopic–geochemical data. *Petrology* **2013**, *21*, 351–374. [CrossRef]

22. Kozlov, N.E.; Sorochtin, N.O.; Glaznev, V.N.; Kozlova, N.E.; Ivanov, A.A.; Kudryashov, N.M.; Martinov, E.V.; Tyuremnov, V.A.; Matyushkin, A.V.; Osipenko, L.G. *Geology of the Archean Baltic Shield*; Nauka: St. Petersburg, Russia, 2006; 345p. (In Russian)

23. Zozulya, D.R.; Bayanova, T.B.; Eby, G.N. Ceology and age of the Late Archean Keivy alkaline Province, Northeastern Baltic Shield. *J. Geol.* **2005**, *113*, 601–608. [CrossRef]

24. Pushkarev, Y.D.; Kravchenko, E.V.; Shestakov, G.I. *Geochronological Benchmarks of the Precambrian of the Kola Peninsula*; Nauka: Leningrad, Russia, 1978; p. 136. (In Russian)

25. Belolipetskii, A.P.; Gaskel'berg, V.G.; Gaskel'berg, L.A.; Antonyuk, E.S.; Il'in, Y.I. *Geology and Geochemistry of the Early Precambrian Metamorphic Complexes of the Kola Peninsula*; Nauka: Leningrad, Russia, 1980; 240p. (In Russian)

26. Pozhilenko, V.I.; Gavrilenko, B.V.; Zhirov, D.V.; Zhabin, S.V. *Geology of Mineral Areas of the Murmansk Region*; KSC RAS: Apatity, Russia, 2002; 360p. (In Russian)

27. Kudryashov, N.M.; Lyalina, L.M.; Apanasevich, E.A. Age of Rare-Metal Pegmatites from the Vasin-Myl'k Deposit (Kola Region): Evidence from U–Pb Geochronology of Microlite. *Dokl. Earth Sci.* **2015**, *461*, 321–3250. [CrossRef]

28. Kudryashov, N.M.; Skublov, S.G.; Galankina, O.L.; Udoratina, O.V.; Voloshin, A.V. Abnormally high-hafnium zircon from rare-metal pegmatites of the Vasin-Mylk deposit (the northeastern part of the Kola Peninsula) // Chemie der Erde. *Geochemistry* **2019**, *6*, 125489. [CrossRef]

29. Kudryashov, N.M.; Mokrushin, A.V. Mesoarchean Gabbroanorthosite Magmatism of the Kola Region: Petrochemical, Geochronological, and Isotope-Geochemical Data. *Petrology* **2011**, *19*, 169–184. [CrossRef]

30. Vrevskii, A.B. Age and sources of the anorthosites of the neoarchean Kolmozero-Voron'ya greenstone belt (Fennoscandian shield). *Petrology* **2016**, *24*, 527–542. [CrossRef]

31. Ostroumov, G.V. *Unified Methods for the Analysis of Silicate Rocks Using Complexonometry*; All-Union Research Institute of Mineral Raw Materials: Moscow, Russia, 1979; 33p. (In Russian)

32. Ronkin, Y.L.; Lepikhina, O.P.; Golik, S.V.; Zhuravlev, D.Z.; Popova, O.Y. *Multielement Analysis of Geological Samples by Acid Decomposition and Termination on HR ICPMS Element 2. Information Digest of Scientific Works of the IGG UB RAS*; IGG UB RAS: Ekaterinburg, Russia, 2005; pp. 423–433. (In Russian)

33. Ireland, T.R. Ion Microprobe Mass-Spectrometry: Techniques and Applications in Cosmochemistry and Geochronology. In *Advances in Analytical Geochemistry*; Hyman, M., Rowe, M., Eds.; JAI Press: London, UK, 1993; Volume 2, pp. 1–118. [CrossRef]

34. Coble, M.A.; Vazquez, J.; Barth, A.P.; Wooden, J.; Burns, D.; Kylander-Clark, A.; Jackson, S.; Vennari, C.E. Trace Element Characterization of MAD-559 Zircon Reference Material for Ion Microprobe Analysis. *Geostand. Geoanalytical Res.* **2018**, *42*, 481–497. [CrossRef]

35. Ludwig, K.R. *SQUID 2: A User's Manual*; Berkeley Geochronology Centre Special Publication: Berkeley, CA, USA, 2009; Volume 5, pp. 1–110.

36. Boynton, W.V. Cosmochemistry of the rare earth elements: Meteorite studies. In *Rare Earth Element Geochemistry*; Henderson, P., Ed.; Elsevier: Amsterdam, The Netherlands, 1984; pp. 63–114.

37. Watson, E.B.; Wark, D.A.; Thomas, J.B. Crystallization thermometers for zircon and rutile. *Contrib. Miner. Pet.* **2006**, *151*, 413–433. [CrossRef]

38. Ludwig, K.R. *Isoplot 3.75, a Geochronological Toolkit for Excel*; Berkeley Geochronology Center Special Publication: Berkeley, CA, USA, 2012; Volume 5, pp. 1–75.

39. Middlemost, E.A.K. Naming materials in the magma/igneous rock system. *Earth-Sci. Rev.* **1994**, *37*, 215. [CrossRef]

40. Wedepohl, K.H. The composition of the continental crust. *Geochim. Cosmochim. Acta* **1995**, *59*, 1217–1232. [CrossRef]

41. Hoskin, P.W.O. Trace-element composition of hydrothermal zircon and the alteration of Hadean zircon from the Jack Hills, Australia. *Geochim. Cosmochim. Acta* **2005**, *69*, 637–648. [CrossRef]

42. Sweetapple, M.T.; Collins, P.L.F. Genetic framework for the classification and distribution of Archean rare metal pegmatites in the North Pilbara Craton, Western Australia. *Econ. Geol.* **2002**, *97*, 873–895. [CrossRef]

43. Zagorsky, V.E.; Vladimirov, A.G.; Makagon, V.M.; Kuznetsova, L.G.; Smirnov, S.Z.; D'yachkov, B.A.; Annikova, I.Y.; Shokal'sky, S.P.; Uvarov, A.N. Large fields of spodumene pegmatites in the settings of rifting and postcollisional shear–pull-apart dislocations of continental lithosphere. *Russ. Geol. Geophys.* **2014**, *55*, 237–251. [CrossRef]

44. Annikova, I.Y.; Vladimirov, A.G.; Smirnov, S.Z.; Gavryushkina, O.A. Geology and Mineralogy of the Alakha Spodumene Granite Porphyry Deposit, Gorny Altai, Russia. *Geol. Ore Depos.* **2016**, *58*, 404–426. [CrossRef]

45. Xiang, W.; Minghua, R.; Jie, C. The muscovite granites: Parental rocks to the Nanling Range tungsten mineralization in South China. *Ore Geol. Rev.* **2017**, *88*, 702–717. [CrossRef]

46. Watson, E.B. Zircon saturation in felsic liquids: Experimental results and applications to trace element geochemistry. *Contrib. Miner. Petrol.* **1979**, *70*, 407–419. [CrossRef]

47. Watson, E.B.; Harrison, T.M. Zircon saturation revisited: Temperature and com-position effects in a variety of crustal magma types. *Earth Planet. Sci. Lett.* **1983**, *64*, 295–304. [CrossRef]

48. Corfu, F.; Hanchar, J.M.; Hoskin, P.W.O.; Kinny, P. Atlas of zircon textures. *Rev. Miner. Geochem.* **2003**, *53*, 469–500. [CrossRef]

49. Rubatto, D. Zircon: The Metamorphic Mineral. *Rev. Miner. Geochem.* **2017**, *83*, 261–295. [CrossRef]

50. Geisler, T.; Seydoux-Guillaume, A.M.; Wiedenbeck, M.; Wirth, R.; Berndt, J.; Zhang, M.; Mihailova, B.; Putnis, A.; Salje, E.K.H.; Schlüter, J. Periodic precipitation pattern formation in hydrothermally treated metamict zircon. *Am. Miner.* **2004**, *89*, 1341–1347. [CrossRef]

51. Nasdala, L.; Kronz, A.; Wirth, R.; Vaczi, T.; Perez-Soba, C.; Willner, A.; Kennedy, A.K. The phenomenon of deficient electron microprobe totals in radiation-damaged and altered zircon. *Geochim. Cosmochim. Acta* **2009**, *73*, 1637–1650.

52. Zamyatin, D.A.; Shchapova, Y.V.; Votyakov, S.L.; Nasdala, L.; Lenz, C. Alteration and chemical U-Th-total Pb dating of heterogeneous high-uranium zircon from a pegmatite from the Aduiskii massif, middle Urals, Russia. *Miner. Pet.* **2017**, *111*, 475–497. [CrossRef]

53. Ewing, R.C.; Meldrum, A.; Wang, L.; Weber, W.J.; Corrales, L.R. Radiation effects in zircon. *Rev. Miner. Geochem.* **2003**, *53*, 387–425. [CrossRef]

54. Geisler, T.; Schaltegger, U.; Tomaschek, F. Re-equilibration of zircon in acqueous fluids and melts. *Elements* **2007**, *3*, 43–50. [CrossRef]

55. Belousova, E.; Griffin, W.; O'Reilly, S.Y.; Fisher, N. Igneous zircon: Trace element composition as an indicator of source rock type. *Contrib. Miner. Pet.* **2002**, *143*, 602–622. [CrossRef]

56. Grimes, C.B.; Wooden, J.L.; Cheadle, M.J.; John, B.E. "Fingerprinting" tectono-magmatic provenance using trace elements in igneous zircon. *Contrib. Miner. Pet.* **2015**, *170*, 46. [CrossRef]

57. Rubatto, D.; Gebauer, D. Use of cathodoluminescence for U–Pb zircon dating by ion microprobe: Some examples from the Western Alps. In *Cathodoluminescence in Geosciences*; Pagel, M., Barbin, V., Blanc, P., Ohnenstetter, D., Eds.; Springer: New York, NY, USA, 2000; pp. 373–400.

58. Schaltegger, U.; Fanning, M.; Günther, D.; Maurin, J.C.; Schulmann, K.; Gebauer, D. Growth, annealing and recrystallization of zircon and preservation of monazite in high-grade metamorphism: Conventional and in-situ U–Pb isotope, cathodoluminescence and microchemical evidence. *Contrib. Miner. Pet.* **1999**, *134*, 186–201. [CrossRef]

59. Rubatto, D. Zircon trace element geochemistry: Distribution coefficients and the link between U–Pb ages and metamorphism. *Chem. Geol.* **2002**, *184*, 123–138. [CrossRef]

60. Watson, E.B.; Harrison, T.M. Zircon thermometer reveals minimum melting conditions on earliest Earth. *Science* **2005**, *308*, 841–844. [CrossRef]

61. Ferry, J.M.; Watson, E.B. New thermodynamic models and revised calibrations for the Ti-in-zircon and Zr-in-rutile thermometers. *Contrib. Miner. Pet.* **2007**, *154*, 429–437. [CrossRef]

62. Myskova, T.A.; Gglebovitsky, V.A.; Mil'kevich, R.I.; Berezhnaya, N.G.; Skublov, S.G. Improvement of composition and age of aluminum gneisses of the Uragubskaya greenstone Later Archaean structure, Kola Peninsula. *Notes Russ. Miner. Soc.* **2010**, *139*, 15–21. (In Russian)

63. Kudryashov, N.M.; Kalinin, A.A.; Lyalina, L.M.; Serov, P.A.; Elizarov, D.V. Gold Occurrences in the Kolmozero-Voronya Archean greenstone belt, Kola region: Geological, mineralogical, geochronological, and isotope-geochemical characteristics. *Lithosphere* **2015**, *6*, 83–100.

64. Balashov, Y.A.; Bayanova, T.B.; Mitrofanov, F.P. Isotope data on the age genesis of layered basic-ultrabasic intrusions in the Kola Peninsula and northern Karelia, northeastern Baltic Shield. *Precambr. Res.* **1993**, *64*, 197–205. [CrossRef]

65. Amelin, Y.V.; Semenov, V.S. Nd and Sr isotopic geochemistry of mafic layered intrusions in the eastern Baltic shield: Implications for the evolution of Paleoproterozoic continental mafic magmas. *Contrib. Miner. Pet.* **1996**, *124*, 255–272. [CrossRef]